Evaluation of 11C-Methionine PET and Anatomic MRI Associations in Diffuse Intrinsic Pontine Glioma

Christopher L. Tinkle[1], Elizabeth C. Duncan[2], Mikhail Doubrovin[3], Yuanyuan Han[4], Yimei Li[4], Hyun Kim[5], Alberto Broniscer[6], Scott E. Snyder[3], Thomas E. Merchant[1], and Barry L. Shulkin[3]

[1]Department of Radiation Oncology, St. Jude Children's Research Hospital, Memphis, Tennessee; [2]University of Tennessee Health Science Center, Memphis, Tennessee; [3]Department of Diagnostic Imaging, St. Jude Children's Research Hospital, Memphis, Tennessee; [4]Department of Biostatistics, St. Jude Children's Research Hospital, Memphis, Tennessee; [5]Department of Radiation Oncology, Washington University, St. Louis, Missouri; and [6]Department of Oncology, University of Pittsburgh Medical Center, Pittsburgh, Pennsylvania

The role of metabolic imaging in the diagnosis, treatment, and response assessment of diffuse intrinsic pontine glioma (DIPG) is poorly defined. We investigated the uptake of 11C-methionine in pediatric patients with newly diagnosed DIPG and evaluated the associations of 11C-methionine PET metrics with conventional MRI indices and survival outcomes. **Methods:** Twenty-two patients with newly diagnosed DIPG were prospectively enrolled on an institutional review board–approved investigational study of 11C-methionine PET. All patients underwent baseline 11C-methionine PET/CT, and initial treatment-response scans after chemotherapy or radiation therapy were obtained for 17 patients. Typical and atypical DIPGs were assessed clinically and radiographically and defined by multidisciplinary consensus. Three-dimensional regions of interest, reviewed by consensus between a nuclear medicine physician and a radiation oncologist, were delineated after coregistration of PET and MR images. Associations of 11C-methionine uptake intensity and uniformity with survival, along with associations between 11C-methionine uptake and conventional MRI tumor indices over time, were evaluated. 11C-methionine PET voxel values within regions of interest were assessed as threshold values across proportions of the study population, and 11C-methionine uptake at baseline was assessed relative to MRI-defined tumor progression. **Results:** 11C-methionine uptake above that of uninvolved brain tissue was observed in 18 of 22 baseline scans (82%) and 15 of 17 initial response scans (88%). 11C-methionine avidity within MRI-defined tumor was limited in extent, with 11 of 18 positive baseline 11C-methionine PET scans (61%) showing less than 25% 11C-methionine–avid tumor. The increase in total tumor volume with 11C-methionine PET was relatively limited (17.2%; interquartile range, 6.53%–38.90%), as was the extent of 11C-methionine uptake beyond the MRI-defined tumor (2.2%; interquartile range, 0.55%–10.88%). Although baseline 11C-methionine PET intensity and uniformity metrics did not correlate with survival outcomes, initial 11C-methionine avidity overlapped with recurrent tumor in 100% of cases. A clinical diagnosis of atypical DIPG was associated with borderline significantly prolonged progression-free survival (P = 0.07), yet 11C-methionine PET indices at diagnosis did not differ significantly between atypical and typical DIPGs. **Conclusion:** Most newly diagnosed DIPGs are successfully visualized by 11C-methionine PET. Baseline 11C-methionine uptake delineates regions at increased risk for recurrence, yet intensity and uniformity metrics did not correlate with treatment outcomes in children with DIPG in this study.

Key Words: 11C-methionine PET; MRI; pediatric; brainstem glioma; DIPG; diffuse midline glioma

Patients with diffuse intrinsic pontine glioma (DIPG) have a stagnant median survival of less than 1 y (1). Despite the recent addition of the "diffuse midline glioma, H3 K27M mutant" histologic entity to the 2016 World Health Organization classification of central nervous system tumors (2), DIPG remains a largely clinical diagnosis based on stereotypic neurologic symptoms of acute onset and characteristic features on conventional MRI (3). Although more routine diagnostic biopsy may be performed at several high-volume centers (4), biopsy is generally reserved in the United States for patients with "atypical" DIPG in which either or both of the above-mentioned clinical or radiologic features are absent or incomplete (5). Primary treatment for DIPG consists of definitive radiation therapy (RT) targeted primarily at the fluid-attenuated inversion recovery (FLAIR) abnormality on diagnostic MRI. However, uncertainties remain concerning the nature and extent of the MRI-defined tumor volume and treatment-response evaluation in DIPG. Conventional MRI remains limited in its ability to differentiate typical from atypical DIPG and to define functionally active disease (6,7).

Metabolic imaging with PET has been widely used for tumor detection and metabolic characterization, target delineation, and treatment-response monitoring of brain tumors. Although 18F-FDG is the most widely used radiotracer for PET imaging and has been evaluated in several studies of pediatric brain stem glioma (8,9), the elevated 18F-FDG uptake in normal brain tissue and at sites of infection or inflammation limits its use (10). Imaging with 11C-methionine has proved useful for several tumors in which 11C-methionine uptake via large amino acid transporter 1 is increased relative to that in surrounding healthy tissues (11,12). Studies on adult brain tumors suggest a role for 11C-methionine PET in prediction of histopathologic tumor grade, target delineation for both diagnostic biopsy and RT planning, prediction of

required RT dose thresholds for tumor control, therapy-response assessment and survival prediction, and differentiation between therapy effects and tumor recurrence (13).

Although PET may provide important insights into the biology of DIPG and its response to therapeutic interventions, investigations of ^{11}C-methionine PET imaging in DIPG have been limited, with most studies conducted in heterogeneous pediatric brain tumor populations (14–17). The objectives of this study were to examine the contribution of the ^{11}C-methionine PET–delineated tumor volume to the conventional MRI-based tumor volume at diagnosis and in the early response to chemotherapy or RT and to assess the prognostic value of baseline ^{11}C-methionine PET metrics in a series of children with newly diagnosed DIPG who were enrolled in a prospective study of ^{11}C-methionine PET.

MATERIALS AND METHODS

Study Description and Patient Population

Between August 2009 and December 2016, 22 pediatric patients with a median age of 9.3 y (range, 6.8–13.5 y) and histologically confirmed or suspected DIPG were enrolled in a prospective protocol (NCT00840047) at St. Jude Children's Research Hospital to evaluate the biodistribution of ^{11}C-methionine in children and young adults with tumors. With the agreement of the primary attending physician and confirmation of known or suspected neoplastic disease, patients were approached for enrollment. The protocol was approved by our institutional review board, and all enrolled subjects gave written informed consent. The current analysis was restricted to patients with newly diagnosed DIPG who underwent ^{11}C-methionine PET and MRI evaluations before the initiation of therapy. All patients were irradiated using conventional fractionation (1.8 Gy per day) to a total dose of 54–55.8 Gy. The categorization of atypical DIPG was reached by consensus on multidisciplinary review of neuroimaging features and clinical symptomatology. Atypical features included prolonged symptom duration before diagnosis, fewer than 2 characteristic neurologic symptoms (cranial nerve deficits, long tract, and cerebellar signs), radiographic features of limited infiltrative growth pattern, eccentricity within the pons (often occupying less than half the pons and with more dorsal growth without significant basilar artery encasement), and more prominent and heterogeneous contrast enhancement (18–20). Of the 22 patients, histologic confirmation of diffuse glioma was obtained in 10 patients (45%) in the form of diagnostic biopsy, resection of distant metastatic disease, or autopsy.

[11]C-Methionine PET Acquisition and Reconstruction

[11]C-methionine was produced starting from ^{11}C-methyl iodide and L-homocysteine thiolactone by the method of Ishiwata et al. (11), as adapted for preparation on a PETChem Solutions automated synthesis module (21). ^{11}C-methionine was administered under an investigational-new-drug authorization. Before undergoing ^{11}C-methionine PET examinations, participants fasted for at least 4 h. They then received intravenous injections of 740 MBq (20 mCi) of ^{11}C-methionine per 1.7 m^2 of body surface area (maximum prescribed dose, 740 MBq). Approximately 5 min later, low-dose transmission CT images for attenuation correction and lesion localization and PET images were obtained using a GE Healthcare Discovery LS PET/CT scanner (before April 2011) or a GE Healthcare Discovery 690 PET/CT scanner. CT acquisition parameters included slice thickness of 0.5 cm, tube rotation of 0.8 s, table speed of 1.5 cm/rotation, pitch of 1.5:1, and 120 kV and 90 mA, with dose modulation. Emission images were acquired for 15 min in 3 dimensions. ^{11}C-methionine PET and CT images were reconstructed in multiple planes using a vendor-supplied 3-dimensional iterative reconstruction algorithm. ^{11}C-methionine PET CT scans were obtained within 2 wk of RT initiation and subsequently at the discretion of the treating physician.

MRI Acquisition

Standard MR images were acquired using a 3.0-T scanner. The imaging protocols included an axial T2-weighted FLAIR sequence (T2FLAIR) (repetition time, 10,000 ms; echo time, 103 ms; flip angle, 130), an axial T1-weighted postgadolinium (T1post) sequence (repetition time, 233 ms; echo time, 2.22 ms; flip angle, 70), and an axial T2-weighted fast spin-echo sequence (repetition time, 7,960 ms; echo time, 83 ms; flip angle, 180). Baseline MRI was performed within 2 wk before RT initiation and at 1- to 3-mo intervals after RT completion in accordance with the therapeutic protocol or at the discretion of the treating physician. The median interval from the end of RT to the first surveillance ^{11}C-methionine PET scan, and between baseline and the first surveillance MRI and ^{11}C-methionine PET scans, were 32.5, 6, and 1 d, respectively (Supplemental Table 1; supplemental materials are available at http://jnm.snmjournals.org).

Image Analysis

MR scans and associated ^{11}C-methionine PET scans were coregistered using standard vendor-supplied software (MIM Software Inc.). The anatomic tumor extent was manually delineated on the basis of T2FLAIR and T1post abnormalities on MRI, and the metabolic tumor volume was delineated on the basis of ^{11}C-methionine avidity by using the validated PET-edge technique in MIM software with manual adjustment in regions approximating the midbrain/basal ganglia because of the inherent increased uptake in those regions (22). Segmented tumor volumes were reviewed by a board-certified radiation oncologist and nuclear medicine physician and defined by consensus.

The SUV$_{max}$ of the tumor was compared with that of the noninvolved left frontal background white matter on ^{11}C-methionine PET scans coregistered with MRI. This choice of background region was based on a desire for reproducibility, its remoteness from the tumor area, and its low probability of having been affected by biopsy. The uptake of ^{11}C-methionine was graded on a scale from 1 to 3, with 1 indicating that uptake was present but less than in noninvolved background white matter, 2 indicating that uptake was approximately equal to background uptake, and 3 indicating that uptake was greater than in the background (Supplemental Fig. 1A). An ^{11}C-methionine PET tumor–to–normal-tissue SUV$_{max}$ index of 1.3 was considered the threshold for malignant activity (23,24), and an intensity score of 3 was considered positive. ^{11}C-methionine uniformity was defined as the percentage of the tumor (as delineated on T2FLAIR MRI) exhibiting ^{11}C-methionine uptake and was graded on a 4-point scale (1, 1%–24%; 2, 25%–49%; 3, 50%–74%; and 4, 75%–100%) (Supplemental Fig. 1B) (25).

Through Boolean operations in MIM, the concordance and discordance between delineated tumor volumes were defined, respectively, as an overlap and a lack of overlap between 2 segmented volumes of interest. The volumes and proportions of tumor representing tumor edema (T2FLAIR), tumor enhancement (T1post), ^{11}C-methionine–avid tumor (^{11}C-methionine PET), and total tumor volume (defined as either the T2FLAIR volume or the union of all 3 volumes, where appropriate) were delineated, and the percentage and quantitative volume in milliliters were assessed relative to the total quantifiable tumor volume. Within identified regions of interest (ROIs), the SUVs per voxel were extracted and the volume and percentage of the total tumor volume across successive SUV intervals from 1 to 5 (in increments of 1.0) were calculated and compared across imaging time points.

Statistical Analysis

The median values, interquartile ranges, and range, count, and frequency measures were summarized by descriptive statistics. Comparisons across ordinal data were made using the Wilcoxon rank-sum test. The signed-rank test was used to evaluate tumor volume change over time. Progression-free survival (PFS) was defined as the time

from RT initiation to progression; that is, to local failure, distant failure, or death, whichever occurred first. Overall survival (OS) was defined as the time from RT initiation to death from any cause. Patients who experienced no event were censored at their last follow-up date. Probability estimates of PFS and OS were calculated by the Kaplan–Meier method and compared using the log-rank test. A Cox proportional hazards model was used to identify imaging and clinicopathologic predictors of PFS and OS distributions. Risk estimates, estimated by hazard ratios and P values, and 95% confidence intervals were reported. Statistical analyses were performed using SAS, version 9.4 (SAS Institute). A P value of less than 0.05 for a 2-sided test was considered statistically significant.

RESULTS

Study Population and Outcomes

Between August 2009 and December 2016, 22 of 154 eligible patients with newly diagnosed DIPG were enrolled and evaluated with ^{11}C-methionine PET and MRI before receiving definitive RT (Supplemental Fig. 2). Enrolled patients underwent subsequent ^{11}C-methionine PET at the discretion of the treating physician, with 17 patients undergoing ^{11}C-methionine PET and MRI at their first post-RT follow-up (Supplemental Table 1). Eight patients were considered to have atypical DIPG, with all but one undergoing MRI-guided stereotactic needle biopsy. Most patients were coenrolled on phase I clinical trials with concurrent or adjuvant systemic therapy. The patient, treatment, and outcome characteristics are summarized in Supplemental Table 2.
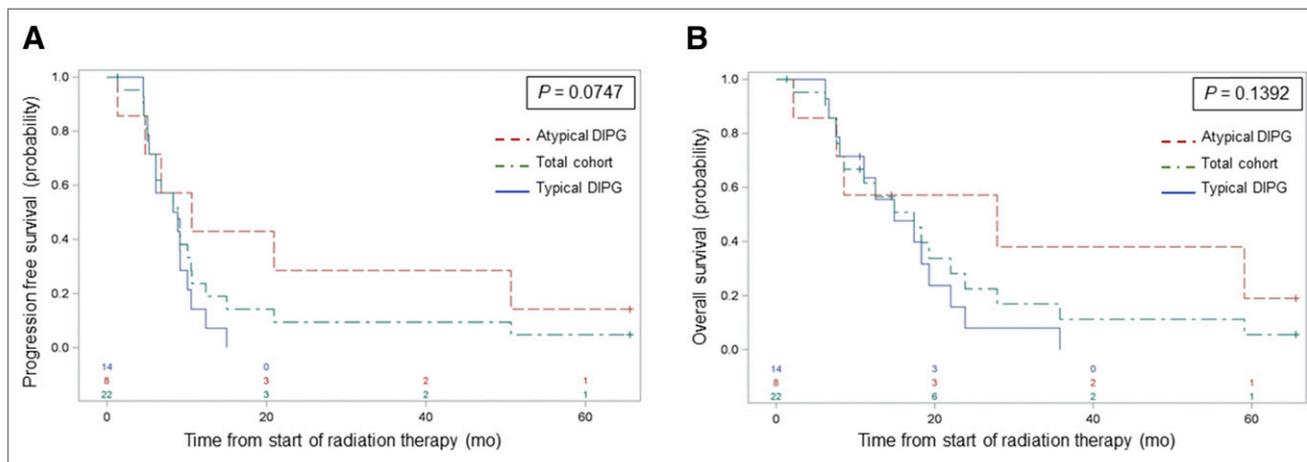
The 6-mo PFS and 12-mo OS rates for the total cohort were 73% (95% confidence interval, 54%–91%) and 63% (95% confidence interval, 43%–84%), respectively (Fig. 1). The OS was significantly longer in patients who underwent ^{11}C-methionine PET imaging than in a contemporary population of 97 patients with newly diagnosed DIPG who were treated at St. Jude but did not undergo ^{11}C-methionine PET ($P = 0.03$) (Supplemental Fig. 3), suggesting a physician bias toward further defining atypical brain stem lesions through investigational ^{11}C-methionine PET imaging. Consistent with this suggestion within the ^{11}C-methionine PET cohort, a trend for significantly prolonged PFS ($P = 0.07$) was observed in patients with atypical versus typical DIPG, whereas no significant difference in OS was observed in this limited cohort (Fig. 1).

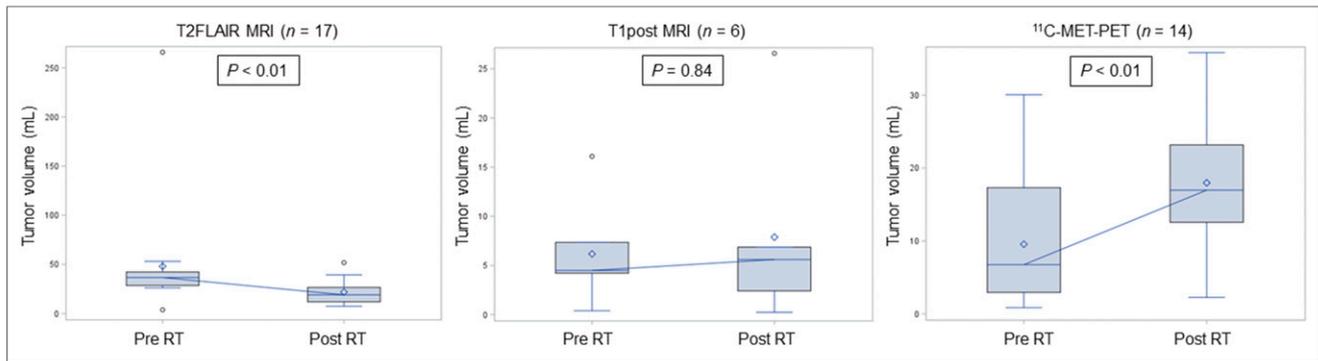### ^{11}C-Methionine PET Metrics and Survival Associations

Scoring of the intensity of ^{11}C-methionine uptake at baseline revealed that the tumors of 18 of 22 patients (82%) exhibited ^{11}C-methionine uptake greater than that of uninvolved brain tissue. Of the 4 patients with negative baseline ^{11}C-methionine uptake, pontine glioblastoma was ultimately diagnosed in two. Conversely, for the 2 patients with biopsy-confirmed pontine low-grade glioma, the baseline ^{11}C-methionine PET scans were positive. Of those patients with positive baseline ^{11}C-methionine PET scans, the extent of ^{11}C-methionine uptake within the MRI-defined tumor volume, or ^{11}C-methionine uniformity, was relatively limited, with 11 of 18 (61%) having positive baseline ^{11}C-methionine PET showing less than 25% ^{11}C-methionine–avid tumor. Interestingly, similar ^{11}C-methionine intensity proportions were observed at the first post-RT imaging, with 15 of 17 patients (88%) having greater ^{11}C-methionine intensity within the MRI-defined tumor than in uninvolved brain. ^{11}C-methionine uniformity was also increased, with 11 of 15 patients (73%) with ^{11}C-methionine PET–positive first surveillance scans showing greater than 50% ^{11}C-methionine–avid tumor compared with 4 of 18 patients (22%) at diagnosis, suggesting that significant decreases in ^{11}C-methionine intensity or extent are not observed acutely with initial ^{11}C-methionine PET imaging after chemotherapy or RT in DIPG. Selected imaging metrics and clinical features are presented in Supplemental Table 3.

Tumor volumes were delineated on T1post, T2FLAIR, and ^{11}C-methionine PET images at diagnosis and first surveillance and were compared over time for those patients with assessable tumor volumes at both time points (Fig. 2; Supplemental Table 4). As observed previously (25), significant reductions in T2FLAIR tumor volumes were noted shortly after RT ($P < 0.01$), whereas abnormal ^{11}C-methionine PET volumes were significantly increased acutely ($P < 0.01$).

The impact of imaging metrics and clinical variables on survival outcomes was assessed through Cox proportional hazards models and, within this dataset, failed to show a significant association of ^{11}C-methionine intensity (uptake in tumor $\leq$ uptake in normal brain vs. $>$ uptake in normal brain) or ^{11}C-methionine uniformity (continuous or $\leq$ 10% vs. $>$ 10% MRI-defined ^{11}C-methionine–avid tumor) (Table 1). Although the presence of enhancement on baseline MRI also failed to significantly influence outcome, patients with typical DIPG had a borderline-significant increase in

FIGURE 1. PFS (A) and OS (B) estimates for total cohort, patients with typical DIPG, and patients with atypical DIPG, showing trend toward significant difference in PFS by DIPG type. CI = confidence interval.

FIGURE 2. Box-and-whisker plots of imaging modality–defined tumor-volume change over time in patients with imaging abnormalities noted at both time points. Significant volume reductions were observed after RT for T2FLAIR MRI–defined tumor and for ^{11}C-methionine PET–defined tumor. Included are medians (connecting horizontal lines), means (diamonds), interquartile ranges (boxes), minimum and maximum values (whiskers), and outliers, that is, values beyond 1.5 interquartile ranges (circles).

the hazard for progression relative to those with an atypical DIPG presentation (hazard ratio, 2.75; $P = 0.06$). ^{11}C-methionine PET intensity or uniformity, as well as tumor enhancement on MRI, were also assessed by DIPG type, and we again observed no significant differences in ^{11}C-methionine PET or conventional MRI metrics at diagnosis for typical and atypical DIPG (data not shown).

The association between baseline ^{11}C-methionine PET avidity and subsequent MRI-based tumor progression volumes was evaluated by delineating 3-dimensional ROIs and assessing the frequency and extent of overlap of the progressive tumor volume and initial ^{11}C-methionine PET volume (Supplemental Fig. 4). Of the patients with initially positive ^{11}C-methionine PET scans who experienced local progression (64%), 100% developed recurrent tumors within the initial ^{11}C-methionine PET–avid volume, with a median proportion of overlap volume of 13.5% (interquartile range, 5.6%–18.9%) relative to the total recurrent volume.

^{11}C-Methionine PET and Conventional MRI Coincidence

To define the extent to which ^{11}C-methionine uptake contributes to conventional MRI in the identification of tumor abnormalities, volumetric ROIs were delineated on baseline and first post-RT ^{11}C-methionine PET and on T1post and T2FLAIR MR images (Fig. 3). By using Boolean operations, we found that ^{11}C-methionine–avid
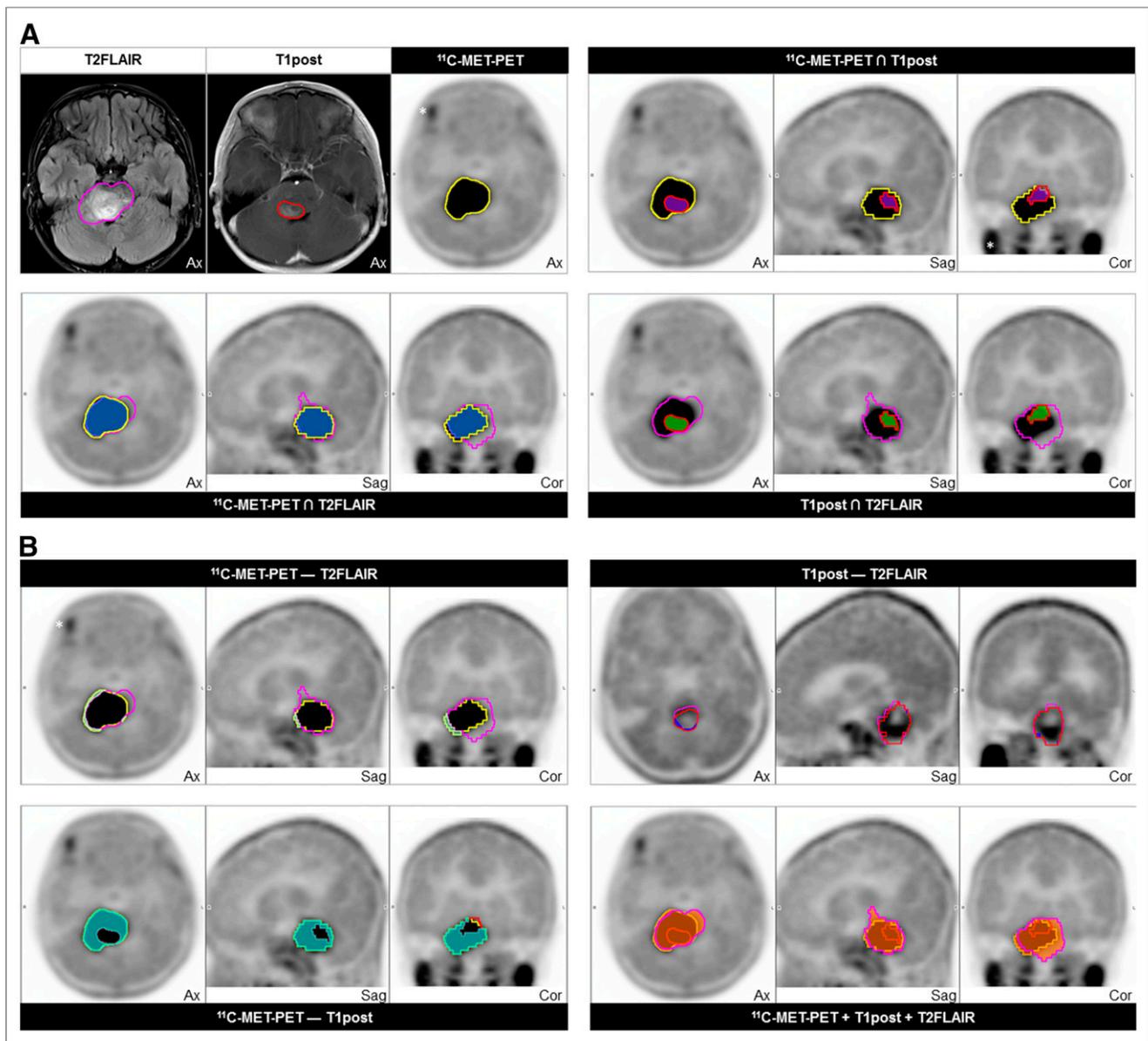
and T2FLAIR abnormality–delineated ROIs at baseline and first imaging follow-up showed the most overlap, or concordance, whereas the most discordant ^{11}C-methionine PET–MRI ROIs at both time-points were ^{11}C-methionine–avid and T1post abnormalities (Figs. 4A and 4B). As expected, T1post abnormalities were rarely observed outside the T2FLAIR abnormalities on diagnostic or first follow-up MR images. Importantly, although 14 of 18 patients exhibited some ^{11}C-methionine PET avidity outside the T2FLAIR abnormality at baseline, this avidity was significantly limited in extent, with a median percentage volume of discordance relative to T2FLAIR volume of 2.2% (interquartile range, 0.55%–10.88%). Additionally, the region of abnormal ^{11}C-methionine uptake increased the total tumor volume (the sum of the T2FLAIR, T1post, and ^{11}C-methionine PET abnormalities) by a relatively small extent (17.2%; interquartile range, 6.53%–38.90%) (Fig. 4C).

^{11}C-Methionine PET SUV Tumor Proportions

To further characterize abnormal ^{11}C-methionine uptake within conventional MRI-defined DIPG tumors, ^{11}C-methionine SUV voxel values within T2FLAIR-defined tumor volumes were obtained and the proportion of tumor volume within a range of SUVs was assessed at baseline and at the first post-RT imaging for each patient (Fig. 5). At diagnosis, most patients had tumor SUVs

TABLE 1
Cox Proportional Hazards Models of Associations of Baseline Covariates with PFS and OS

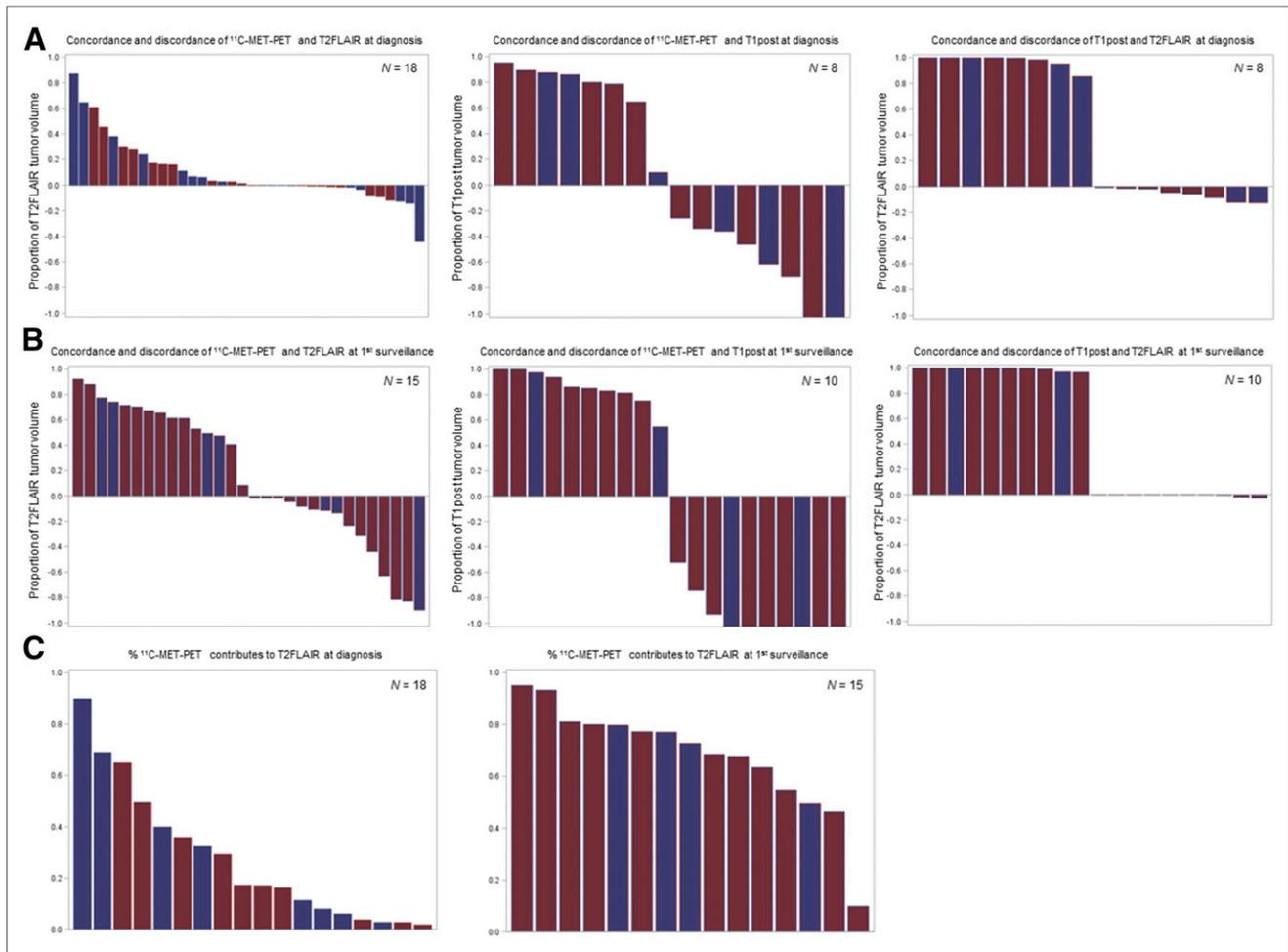| Variable	Survival type	Hazard ratio	P
Contrast enhancement (yes vs. no)	PFS	1.11	0.83
	OS	1.86	0.23
DIPG status (typical vs. atypical)	PFS	2.75	0.06
	OS	2.36	0.13
^{11}C-methionine PET intensity grade (1 and 2 vs. 3)	PFS	1.62	0.43
	OS	1.64	0.42
^{11}C-methionine PET uniformity grade			
Continuous	PFS	1.02	0.23
	OS	1.02	0.20
≤10% vs. >10%	PFS	0.59	0.32
	OS	0.52	0.26

FIGURE 3. Example of concordant and discordant segmented tumor volumes based on T2FLAIR (magenta) and T1post (red) abnormalities on MR images and ^{11}C-methionine abnormality (yellow) on ^{11}C-methionine PET. (A) Concordance volumes with coregistered MRI- and ^{11}C-methionine PET–defined tumor (upper left) and indicated concordance volumes (blue = ^{11}C-methionine PET ∩ T2FLAIR; purple = ^{11}C-methionine PET ∩ T1post; green = T1post ∩ T2FLAIR). (B) Indicated discordance volumes (light green = ^{11}C-methionine PET – T2FLAIR; aqua = ^{11}C-methionine PET – T1post; dark blue = T1post – T2FLAIR) and concordant total tumor volume delineated on MRI and ^{11}C-methionine PET (red-orange, bottom right). *Physiologic uptake in exocrine glands.

between 0 and 2, with the proportion of tumor with these lower SUVs having a relatively broad distribution. However, the initial posttreatment SUV volumes demonstrated a shift to higher SUVs within more limited tumor volumes across patients.

DISCUSSION

This study was undertaken to evaluate the utility of PET imaging with radiolabeled methionine in pediatric patients with newly diagnosed DIPG. We have demonstrated that ^{11}C-methionine uptake is markedly greater within the tumor than in noninvolved white matter, with 82% of enrolled patients (18/22) having been successfully visualized with ^{11}C-methionine PET at diagnosis.

Within the limited longitudinal imaging studies of this cohort, ^{11}C-methionine uptake, as assessed by the frequency of positive ^{11}C-methionine scans and the volumetric proportions of the MRI-defined tumor, increased at the first surveillance imaging after irradiation. Although some PET studies of adult patients with glioma have found reduced ^{11}C-methionine uptake soon after RT, there was considerable heterogeneity in the timing of the post-RT imaging (26). Given the similar post-RT increases in ^{11}C-methionine avidity in pediatric patients with supratentorial high-grade glioma (27), the utility of short-interval ^{11}C-methionine PET imaging for assessing treatment response after irradiation is suspect. The observed slight elevation in methionine uptake after RT is most

FIGURE 4. Waterfall plot of concordance and discordance of imaging modality–defined tumor volumes at diagnosis (A) and first surveillance (B) and contribution of ^{11}C-methionine PET volume to T2FLAIR-defined tumor volume at defined time points (C). Blue = typical DIPG; red = atypical DIPG; MET = methionine.

likely due to radiation-induced inflammation or radiation necrosis, although residual/progressive tumor may also contribute. To further delineate the pathophysiology involved will require posttherapy tumor biopsy or additional follow-up methionine studies in patients with DIPG.

PET imaging with ^{18}F-FDG in pediatric patients with brain stem glioma suggests that those patients with more extensive ^{18}F-FDG uptake within the MRI-defined tumor volume may have a poorer PFS, yet neither ^{18}F-FDG intensity nor histogram metrics of skewness or kurtosis were associated with survival (25,28). This is in distinction to our observations, which did not demonstrate a statistically significant correlation between either ^{11}C-methionine uniformity or intensity and outcome. This lack of correlation may be explained by that fact that ^{11}C-methionine uniformity was limited, with only 16.7% of patients with ^{11}C-methionine uptake of 50% or more within the tumor, compared with 42.5% of patients with this extent of ^{18}F-FDG uptake in a cohort with DIPG (25). An additional point of consideration is the inherent limitation of our relatively few study patients, which may further complicate statistical inferences. Despite this limitation, this report represents the largest prospective study of this important neurooncology radiotracer within a disease diagnosed primarily radiographically, and thus, whereas many findings may be more descriptive in nature, these results represent an important benchmark in the role of L-type amino acid transporter–based PET imaging in pediatric brain stem glioma. Looking forward, given the specialized radiochemistry required for, and the short half-life associated with, ^{11}C-methionine, an additional L-type amino acid transporter–based radiotracers that may warrant evaluation in this population is ^{18}F-FDOPA (29). The use of integrated PET/MRI scanners to better synergize the complementary anatomic and biologic information obtained with both modalities and to facilitate rapid image acquisition while minimizing patient variation may also help mitigate some of the current limitations of PET imaging (30).

Uniquely, this study included a larger proportion of patients with atypical presentations of DIPG. We hypothesize that, given the selective enrollment procedures of this clinical trial, these patients were preferentially enrolled in the hope of gaining additional radiographic insight after discordant features were observed on conventional MRI. The distinction between atypical and typical DIPG based on MRI is subjective and often inconsistently defined (6), and there is hope that advanced imaging techniques might better distinguish these entities. Even though most patients with atypical DIPG were ultimately found to have high-grade glioma, we consider this limited sample to have prognostic relevance in view of the trend for significantly longer PFS in these patients.

% Volume	SUV 0~1	1~2	2~3	3~4	4~5
Diagnosis					
1%~25%	22%	28%	22%	22%	
25%~50%	22%	17%	17%	0%	
50%~75%	17%	33%	6%	0%	
75%~100%	17%	17%	0%	0%	
1st Surveillance					
1%~25%	60%	13%	40%	33%	7%
25%~50%	0%	27%	33%	7%	0%
50%~75%	7%	27%	7%	0%	0%
75%~100%	7%	33%	0%	0%	0%
1st Surveillance Minus Diagnosis					
1%~25%	38%	-14%	18%	11%	7%
25%~50%	-22%	10%	17%	7%	0%
50%~75%	-10%	-7%	1%	0%	0%
75%~100%	-10%	17%	0%	0%	0%

Colorimetric scale: -100%, -75%, -50%, -25%, 0%, 25%, 50%, 75%, 100%

FIGURE 5. Descriptive analysis of tumor volume–SUV proportions over indicated time points. Percentage of tumor volume in quartiles with SUV greater than or equal to specified SUV range is displayed with percentage of patients within each SUV range who had indicated volume–SUV relationships. Matrix subtraction of volume–SUV proportions between first surveillance and diagnosis are displayed on bottom row. Colorimetric scale (far right) uses progressively darker red values to indicate relative increase in percentage of patients' specified volume–SUV metrics, whereas progressively darker green values indicate decrease.

Having said that, our analysis of the data revealed no significant correlations between DIPG clinical types and ^{11}C-methionine PET metrics, including baseline ^{11}C-methionine PET intensity and uniformity indices and the coincidence patterns of ^{11}C-methionine PET and MRI-defined tumor volumes. Further studies including more patients and incorporating molecular pathology and multiparametric MR imaging are needed to better evaluate the utility of advanced imaging in defining this important distinction.

Tumor delineation using ^{11}C-methionine PET imaging has been evaluated in the context of conventional imaging modalities in several studies in adults with supratentorial glioma, with some studies finding frequent discordance between the biologically defined ^{11}C-methionine PET tumor and the anatomically defined tumor (24,31). In one study of 39 adults with resected malignant glioma, the region of ^{11}C-methionine uptake in most patients extended beyond the areas of abnormal enhancement and hyperintensity on T1-weighted postcontrast and T2-weighted MRI, respectively (32). However, when an isotropic clinical target volume expansion of 2 cm surrounding the T2-weighted MRI hyperintensity was used for RT planning, 2 separate studies of resected glioma demonstrated that the ^{11}C-methionine–avid regions were completely encompassed in most of the study patients (24,31). In our study, whereas the ^{11}C-methionine PET–delineated tumor extended beyond the T2FLAIR abnormality in most patients at diagnosis, discordant ^{11}C-methionine–avid volumes were generally limited. Although similar PET studies of pediatric infiltrative brain stem tumors are currently lacking, a study of pediatric supratentorial glioma suggested that the extent of ^{11}C-methionine avidity beyond the FLAIR abnormality was similarly limited (27). The distinct molecular alterations in pediatric supratentorial and brain stem high-grade glioma (33) might account, in part, for the observed discrepancies in ^{11}C-methionine PET and MRI coincidence between adult and pediatric gliomas.

We have also shown that ^{11}C-methionine PET might provide important information concerning heterogeneous tumor regions at the highest risk of treatment failure by demonstrating a correlation between the location of increased preradiation ^{11}C-methionine PET activity and the subsequent region of local tumor progression. Studies in adults with glioblastoma have also demonstrated that regions showing elevated ^{11}C-methionine uptake before concurrent chemotherapy or RT predict areas of subsequent failure and have found altered treatment-failure patterns related to the high-dose RT field in a small subset of patients in whom there was ^{11}C-methionine avidity outside the MRI-targeted tumor volume (34). Furthermore, the extent of ^{11}C-methionine uptake in adult patients with high-grade glioma has been associated with poor local tumor control, with one study suggesting that the optimal RT dose necessary for local tumor control could be determined in relation to the level of ^{11}C-methionine uptake on a case-by-case basis (35). Further prospective studies of ^{11}C-methionine PET in pediatric high-grade glioma are needed to evaluate the utility of ^{11}C-methionine PET–based biologic target volume delineation and the reliability of identifying tumor subregions at the highest risk of local progression.

CONCLUSION

Most newly diagnosed DIPGs can be successfully visualized by ^{11}C-methionine PET, with approximately 80% of such tumors having uptake greater than that of normal brain, whereas early post-RT imaging appears to add little to the treatment-response assessment. We observed abnormal ^{11}C-methionine avidity beyond the conventional MRI-defined tumor in most patients, but its extent was limited. Although ^{11}C-methionine PET indices did not appear to differ between typical and atypical DIPG or predict outcomes in this study, the initial regions of abnormal ^{11}C-methionine uptake appear to be predictive for subsequent tumor progression. Larger prospective studies are needed to better define the role of metabolic tumor imaging via ^{11}C-methionine PET in the diagnosis and prognostication of what is becoming a tumor defined by mutation rather than by clinical findings alone.

DISCLOSURE

ACKNOWLEDGMENTS

REFERENCES

1. Jansen MH, Veldhuijzen van Zanten SE, Sanchez Aliaga E, et al. Survival prediction model of children with diffuse intrinsic pontine glioma based on clinical and radiological criteria. *Neuro Oncol.* 2015;17:160–166.
2. Louis DN, Perry A, Reifenberger G, et al. The 2016 World Health Organization classification of tumors of the central nervous system: a summary. *Acta Neuropathol (Berl).* 2016;131:803–820.
3. Warren KE. Diffuse intrinsic pontine glioma: poised for progress. *Front Oncol.* 2012;2:205.
4. Puget S, Beccaria K, Blauwblomme T, et al. Biopsy in a series of 130 pediatric diffuse intrinsic pontine gliomas. *Childs Nerv Syst.* 2015;31:1773–1780.

5. Kaye EC, Baker JN, Broniscer A. Management of diffuse intrinsic pontine glioma in children: current and future strategies for improving prognosis. *CNS Oncol.* 2014;3:421–431.

6. Hankinson TC, Campagna EJ, Foreman NK, Handler MH. Interpretation of magnetic resonance images in diffuse intrinsic pontine glioma: a survey of pediatric neurosurgeons. *J Neurosurg Pediatr.* 2011;8:97–102.

7. Hargrave D, Chuang N, Bouffet E. Conventional MRI cannot predict survival in childhood diffuse intrinsic pontine glioma. *J Neurooncol.* 2008;86:313–319.

8. Goda JS, Dutta D, Raut N, et al. Can multiparametric MRI and FDG-PET predict outcome in diffuse brainstem glioma? A report from a prospective phase-II study. *Pediatr Neurosurg.* 2013;49:274–281.

9. Zukotynski K, Fahey F, Kocak M, et al. ^{18}F-FDG PET and MR imaging associations across a spectrum of pediatric brain tumors: a report from the Pediatric Brain Tumor Consortium. *J Nucl Med.* 2014;55:1473–1480.

10. Goldman S, Pirotte BJ. Brain tumors. *Methods Mol Biol.* 2011;727:291–315.

11. Ishiwata K, Ido T, Abe Y, Matsuzawa T, Iwata R. Tumor uptake studies of S-adenosyl-L-[methyl-^{11}C]methionine and L-[methyl-^{11}C]methionine. *Int J Rad Appl Instrum B.* 1988;15:123–126.

12. Okubo S, Zhen HN, Kawai N, Nishiyama Y, Haba R, Tamiya T. Correlation of L-methyl-^{11}C-methionine (MET) uptake with L-type amino acid transporter 1 in human gliomas. *J Neurooncol.* 2010;99:217–225.

13. Palanichamy K, Chakravarti A. Diagnostic and prognostic significance of methionine uptake and methionine positron emission tomography imaging in gliomas. *Front Oncol.* 2017;7:257.

14. Pirotte BJ, Lubansu A, Massager N, Wikler D, Goldman S, Levivier M. Results of positron emission tomography guidance and reassessment of the utility of and indications for stereotactic biopsy in children with infiltrative brainstem tumors. *J Neurosurg.* 2007;107(suppl)392–399.

15. Rosenfeld A, Etzl M, Bandy D, et al. Use of positron emission tomography in the evaluation of diffuse intrinsic brainstem gliomas in children. *J Pediatr Hematol Oncol.* 2011;33:369–373.

16. Sörensen J, Savitcheva II, Engler H, Langstrom B. 3. Utility of PET and ^{11}C-methionine in paediatric brain tumors. *Clin Positron Imaging.* 2000;3:157.

17. Utriainen M, Metsahonkala L, Salmi TT, et al. Metabolic characterization of childhood brain tumors: comparison of ^{18}F-fluorodeoxyglucose and ^{11}C-methionine positron emission tomography. *Cancer.* 2002;95:1376–1386.

18. Freeman CR, Bourgouin PM, Sanford RA, Cohen ME, Friedman HS, Kun LE. Long term survivors of childhood brain stem gliomas treated with hyperfractionated radiotherapy: clinical characteristics and treatment related toxicities. The Pediatric Oncology Group. *Cancer.* 1996;77:555–562.

19. Kwon JW, Kim IO, Cheon JE, et al. Paediatric brain-stem gliomas: MRI, FDG-PET and histological grading correlation. *Pediatr Radiol.* 2006;36:959–964.

20. Jackson S, Patay Z, Howarth R, et al. Clinico-radiologic characteristics of long-term survivors of diffuse intrinsic pontine glioma. *J Neurooncol.* 2013;114:339–344.

21. Vavere AL, Snyder SE. Synthesis of L-[methyl-^{11}C] methionine ([^{11}C]MET). In: Scott P, Hockley B, eds. *Radiochemical Syntheses.* New York, NY: John Wiley and Sons; 2012:199–212.

22. Lapa C, Linsenmann T, Monoranu CM, et al. Comparison of the amino acid tracers ^{18}F-FET and ^{18}F-DOPA in high-grade glioma patients. *J Nucl Med.* 2014;55:1611–1616.

23. Lilja A, Bergstrom K, Hartvig P, et al. Dynamic study of supratentorial gliomas with L-methyl-^{11}C-methionine and positron emission tomography. *AJNR Am J Neuroradiol.* 1985;6:505–514.

24. Matsuo M, Miwa K, Tanaka O, et al. Impact of [^{11}C]methionine positron emission tomography for target definition of glioblastoma multiforme in radiation therapy planning. *Int J Radiat Oncol Biol Phys.* 2012;82:83–89.

25. Zukotynski KA, Fahey FH, Kocak M, et al. Evaluation of ^{18}F-FDG PET and MRI associations in pediatric diffuse intrinsic brain stem glioma: a report from the Pediatric Brain Tumor Consortium. *J Nucl Med.* 2011;52:188–195.

26. Nariai T, Tanaka Y, Wakimoto H, et al. Usefulness of L-[methyl-^{11}C] methionine-positron emission tomography as a biological monitoring tool in the treatment of glioma. *J Neurosurg.* 2005;103:498–507.

27. Lucas JT Jr, Serrano N, Kim H, et al. ^{11}C-methionine positron emission tomography delineates non-contrast enhancing tumor regions at high risk for recurrence in pediatric high-grade glioma. *J Neurooncol.* 2017;132:163–170.

28. Zukotynski KA, Vajapeyam S, Fahey FH, et al. Correlation of ^{18}F-FDG PET and MRI apparent diffusion coefficient histogram metrics with survival in diffuse intrinsic pontine glioma: a report from the Pediatric Brain Tumor Consortium. *J Nucl Med.* 2017;58:1264–1269.

29. Walter F, Cloughesy T, Walter MA, et al. Impact of 3,4-dihydroxy-6-^{18}F-fluoro-L-phenylalanine PET/CT on managing patients with brain tumors: the referring physician's perspective. *J Nucl Med.* 2012;53:393–398.

30. Pichler BJ, Kolb A, Nagele T, Schlemmer HP. PET/MRI: paving the way for the next generation of clinical multimodality imaging applications. *J Nucl Med.* 2010;51:333–336.

31. Mahasittiwat P, Mizoe JE, Hasegawa A, et al. l-[Methyl-^{11}C] methionine positron emission tomography for target delineation in malignant gliomas: impact on results of carbon ion radiotherapy. *Int J Radiat Oncol Biol Phys.* 2008;70:515–522.

32. Grosu AL, Weber WA, Riedel E, et al. L-(methyl-^{11}C) methionine positron emission tomography for target delineation in resected high-grade gliomas before radiotherapy. *Int J Radiat Oncol Biol Phys.* 2005;63:64–74.

33. Paugh BS, Qu C, Jones C, et al. Integrated molecular genetic profiling of pediatric high-grade gliomas reveals key differences with the adult disease. *J Clin Oncol.* 2010;28:3061–3068.

34. Lee IH, Piert M, Gomez-Hassan D, et al. Association of ^{11}C-methionine PET uptake with site of failure after concurrent temozolomide and radiation for primary glioblastoma multiforme. *Int J Radiat Oncol Biol Phys.* 2009;73:479–485.

35. Iuchi T, Hatano K, Uchino Y, et al. Methionine uptake and required radiation dose to control glioblastoma. *Int J Radiat Oncol Biol Phys.* 2015;93:133–140.